Chemical Science

ROYAL SOCIETY OF CHEMISTRY

EDGE ARTICLE

View Article Online
View Journal | View Issue

Cite this: *Chem. Sci.*, 2024, **15**, 5268

All publication charges for this article have been paid for by the Royal Society of Chemistry

Received 26th October 2023
Accepted 26th February 2024

DOI: 10.1039/d3sc05724k

rsc.li/chemical-science

Nanoscale solvent organization in metal–organic framework ZIF-8 probed by EPR of flexible β-phosphorylated nitroxides†

Artem S. Poryvaev,[a] Aleksandr A. Efremov,[ab] Dmitry V. Alimov,[ab] Kristina A. Smirnova,[ab] Daniil M. Polyukhov,[a] Renad Z. Sagdeev,[a] Samuel Jacoutot,[c] Sylvain R. A. Marque *[c] and Matvey V. Fedin *[ab]

Metal–organic frameworks (MOFs) draw increasing attention as nanoenvironments for chemical reactions, especially in the field of catalysis. Knowing the specifics of MOF cavities is decisive in many of these cases; yet, obtaining them *in situ* remains very challenging. We report the first direct assessment of the apparent polarity and solvent organization inside MOF cavities using a dedicated structurally flexible spin probe. A stable β-phosphorylated nitroxide radical was incorporated into the cavities of a prospective MOF ZIF-8 in trace amounts. The spectroscopic properties of this probe depend on local polarity, structuredness, stiffness and cohesive pressure and can be precisely monitored by Electron Paramagnetic Resonance (EPR) spectroscopy. Using this approach, we have demonstrated experimentally that the cavities of bare ZIF-8 are sensed by guest molecules as highly non-polar inside. When various alcohols fill the cavities, remarkable self-organization of solvent molecules is observed leading to a higher apparent polarity in MOFs compared to the corresponding bulk alcohols. Accounting for such nanoorganization phenomena can be crucial for optimization of chemical reactions in MOFs, and the proposed methodology provides unique routes to study MOF cavities inside *in situ*, thus aiding in their various applications.

1. Introduction

Metal–organic frameworks (MOFs) are inorganic–organic hybrid materials containing metal nodes, such as ions or clusters, interconnected by organic ligands *via* coordination bonds.[1] This class of materials has impressive sensing,[2–4] adsorption and catalytic properties and demonstrates high potential for industrial applications.[5–8] Zeolitic Imidazolate Frameworks (ZIFs) represent one highly prospective class of MOFs.[9–11] ZIFs have a topology similar to zeolites and contain metal ions such as Zn^{2+} or Co^{2+}, as well as imidazolate linkers.[12] ZIF-8 is the most studied member of this family and demonstrates high thermal and hydrothermal stability,[13] structural flexibility,[14,15] and excellent sorption and separation properties.[16–19] The combination of large cavities (~11 Å) interconnected by flexible windows (effective diameter 3.4–7.5 Å (ref. 20)) with a hydrophobic inner surface makes ZIF-8 a material of choice for various sorption and separation applications. Therefore, a hydrophobic nature of the ZIF-8 inner surface is one of the key properties for gas sorption, oil sorption and alcohol separation.[21–26] Despite this, the data on properties of the inner surface of ZIF-8 cavities are scarce in the literature, being limited only to theoretical suggestions and conclusions derived from sorption experiments.[23,27]

Electron Paramagnetic Resonance (EPR) is a powerful method for studying coordination compounds. Its applications to MOFs are currently expanding, mostly focusing on the properties of MOFs such as sorption,[28–31] structural flexibility[32–36] and catalysis.[37–39] Since most of the MOFs are diamagnetic, the application of EPR requires incorporation of some paramagnetic species into the MOFs. Owing to the high sensitivity of EPR, this can be done in trace amounts (1 paramagnetic center per 1000 cavities or less), not disturbing the original structure of the framework. One of the ways to incorporate paramagnetic reporters into MOFs relies on post-synthetic sorption of paramagnetic probes such as 2,2,6,6-tetramethyl(piperidin-1-yl)oxyl (TEMPO),[35,36,40,41] nitrogen monoxide[32] or nitrogen dioxide.[42] This approach is commonly called a method of spin probes. Previously, this method with a TEMPO probe was applied for monitoring gas adsorption on a ZIF-8 surface.[41] Later on, a very fruitful modification has been proposed, called the method of encapsulated spin probes, where nitroxide (TEMPO) radicals were permanently entrapped in the cavities of a MOF (TEMPO@MOF) and used as reporters

[a]*International Tomography Center SB RAS, Novosibirsk, 630090, Russia. E-mail: mfedin@tomo.nsc.ru*

[b]*Novosibirsk State University, Novosibirsk, 630090, Russia*

[c]*Aix Marseille University, CNRS, UMR, Avenue Escadrille Normandie-Niemen, 7273 Marseille, 13397 CEDEX 20, France. E-mail: sylvain.marque@univ-amu.fr*

† Electronic supplementary information (ESI) available. See DOI: https://doi.org/10.1039/d3sc05724k

located exclusively in the cavities (not on the outer surface) of the MOF. This method allows numerous applications, including precise measurements of the window sizes *vs.* temperature,[43] adjusting conditions for various separations.[44,45] assessing pressure effects and aiding in the formation of MOF pellets and composites.[46–50] All information obtained using TEMPO@MOF systems relied on the sensitivity of the EPR spectrum to the presence of oxygen or solvent molecules in the cavity, as well as to the integrity of MOF cavities. However, this TEMPO-based approach provides only basic information on the properties of MOF cavities inside and their changes upon adsorption of various guests.

In a recent series of studies, β-phosphorylated nitroxide radicals were successfully employed to study the local polarity and composition of various solutions.[51–55] The hyperfine interaction (HFI) constants on nitrogen and phosphorus nuclei were found to be extremely sensitive to local polarity, structuredness, stiffness and cohesive pressure, and could be deduced from continuous wave (CW) EPR experiments in solution at ambient temperatures.

In this work, we combined these two independent research studies and incorporated a β-phosphorylated nitroxide into a ZIF-8 cavity as a probe of local polarity. The application of EPR to this system allowed the first direct assessment of the polarity inside the ZIF-8 cavity and its guest-induced changes. Moreover, when ZIF-8 was impregnated with alcohols, the polarity sensed by the probe was found anomalous, in some cases exceeding the bulk polarity of the same solvent, to be assigned to specific guest–host interactions of alcohols with the ZIF-8 inner surface. Below we describe the developed methodology, obtained results and important conclusions obtained from these studies.

2. Experimental section

2.1. Materials

All solvents were used in HPLC grade quality. All reagents and solvents were purchased from commercial sources and used as received without further purification. Nitroxide S1 was prepared as already reported.[55]

2.2. Synthesis of ZIF-8 with encapsulated radicals

We used the same procedure for incorporation of radical S1 into ZIF-8 as that developed previously for incorporation of TEMPO.[43] 0.135 g of anhydrous $ZnCl_2$ (1.0 mmol) was dissolved in 4 ml of deionized water, and then it was added to a solution of the radical with 2-methylimidazole (HMeIm). S1/HMeIm solution was prepared by dissolving 4.92 g of HMeIm (0.06 mol) in 36 ml of deionized water and adding 0.005 mmol of β-phosphorylated nitroxide to the solution. The final molar composition of the synthesis solution was Zn^{2+} : HMeIm : radical : water = 1 : 60 : 0.005 : 2228. The mixture was stirred at room temperature for 6 days. Then S1@ZIF-8 suspension was centrifuged and washed three times with deionized water and five times with methanol. The product was first dried for 24 h at room temperature, and then under reduced pressure at 333 K for the next 24 hours. As a result, we have obtained samples denoted below as "dry" S1@ZIF-8. In all samples there was 1 radical per ~400 MOF cavities (with the average radical–radical distance being ~7–8 nm).

2.3. EPR measurements

EPR studies were performed using a commercial Bruker Elexsys E580 X/Q-band EPR spectrometer equipped with an Oxford Instruments temperature control system (T = 4–300 K) at the Center of Collective Use "Mass spectrometric investigations" SB RAS. In all cases powdered samples were placed into quartz sample tubes (OD = 2.8 mm or 3.8 mm), and the sample height varied between 0.2 and 0.8 cm. S1 solutions in organic solvents were degassed using the following procedure. An EPR tube with 50 μl of solution was frozen in liquid nitrogen and evacuated (to pressure ~0.1 mbar). Then this tube with a sample was filled with argon and heated to room temperature. This procedure was repeated 3 times. S1@ZIF-8 was measured under ambient conditions or under evacuation with a residual pressure of around 10^{-5} mbar. CW EPR spectra were recorded under conditions avoiding unwanted modulation broadening and microwave saturation. For all simulations the EasySpin toolbox for Matlab was used.[56]

2.4. PXRD measurements

Powder X-ray diffraction (PXRD) data were collected on a Pow-Dix 600 (ADANI) diffractometer equipped with a MYTHEN2 R 1D (Dectris) detector at room temperature using Cu Kα radiation at a scanning speed on θ of 0.01° s^{-1}. The samples were placed in an aluminum sample holder. The experimental PXRD patterns agree with the simulated ones from the structures solved by single-crystal XRD data, indicating good crystal phase purity.

3. Results and discussion

3.1. Polarity of bare ZIF-8 cavities

β-Phosphorylated nitroxide S1 (Fig. 1) was selected to probe the internal surface of the ZIF-8 cavities in this study.

The conformation of this radical and, correspondingly, observed HFI splitting strongly depend on the polarity of surrounding media and characteristics such as structuredness, stiffness and cohesive pressure of the surrounding solvent.[51–55]

First we have ensured that the radicals in the synthesized S1@ZIF-8 material are encapsulated (permanently entrapped) inside the cavities of the MOF. For this sake we confirmed the formation of the ZIF-8 material using PXRD (Fig. S1, ESI†) and studied radical behavior by EPR (Fig. 2). The radicals in ZIF-8 demonstrate fast motion EPR spectra characteristics of unrestricted rotation in the cavity (Fig. 2). These spectra remain unchanged upon evacuation with heating, as well as upon flushing with ethanol. Consequently, once these radicals entered the cavities during synthesis, they cannot exit outside due to their large size compared to inter-cavity windows. The room-temperature EPR spectrum of S1@ZIF-8 features a single fraction with narrow lines, meaning that the radical is evenly distributed over the volume of the MOF.

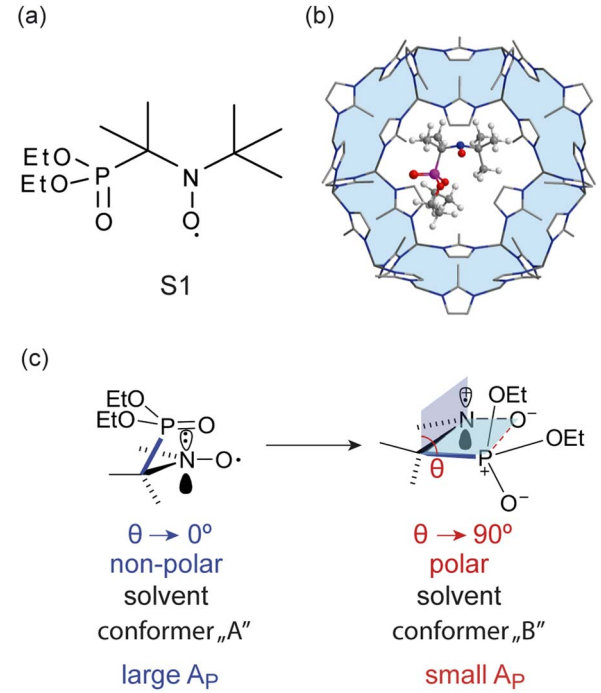

Fig. 1 (a) Structure of β-phosphorylated nitroxide radical S1. (b) The scheme of S1@ZIF-8. (c) Conformational change due to rotation around the C–N bond corresponding to transition from non-polar to polar solvent. Dotted lines illustrate dipole–dipole interactions NO⋯PO.

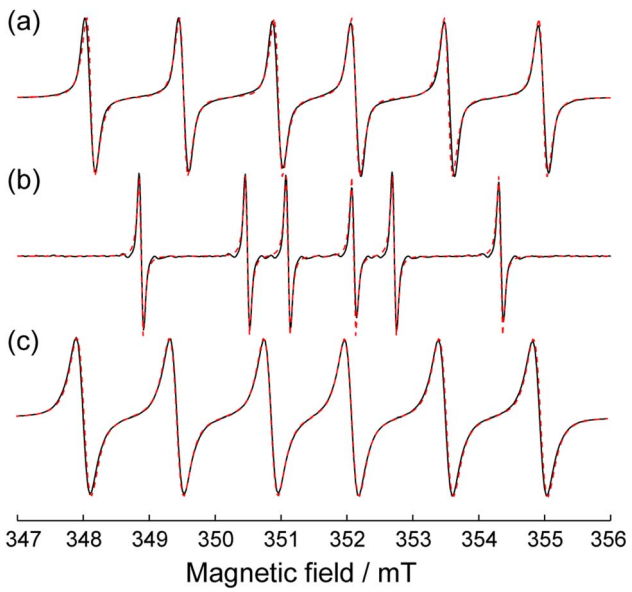

Fig. 2 Room-temperature X-band CW EPR spectra of evacuated (10–5 mbar) S1@ZIF-8 (a) and S1 dissolved in water (b) or *n*-pentane (c). Experimental spectra are shown as solid black lines and simulations as dotted red lines.

Fig. 2 compares the CW EPR spectra of S1 dissolved in water and S1@ZIF-8. The simulation of experimental data shown in Fig. 2 allows obtaining the following set of isotropic HFI constants on nitrogen (A_N) and β-phosphorus (A_P) nuclei (Table 1). The HFIs of this radical were obtained previously in a large set of solvents.[51] Our results in water (A_N = 1.612 mT and A_P = 2.231 mT) agree with previous data within an accuracy of ±0.04 and ±0.05 mT for A_N and A_P, respectively (these values can serve as estimates of measurement error). The spectra in water and in ZIF-8 are markedly different, owing to the different values of A_N and A_P. Both HFIs of these radicals are sensitive to the polarity of the media,[51–55] and the changes of their values between water and the ZIF-8 interior indicate stronger hydrophobicity of the latter. Previous studies have also demonstrated that A_N and A_P show opposite trends *vs.* normalized Reichard polarity constants (E_N^T): A_N moderately grows with E_N^T, whereas A_P strongly decreases upon polarity increase. The obtained HFIs for S1@ZIF-8 (A_N = 1.420 mT and A_P = 4.033 mT) are very close to the values obtained for S1 in *n*-pentane (A_N = 1.430 mT and A_P = 4.100 mT), meaning that the polarity sensed by a probe inside bare ZIF-8 is approximately as small as in *n*-pentane. Interestingly, however, that both A_N and A_P values are slightly lower in ZIF-8 than in *n*-pentane, while one would expect differences of the opposite sign. This might indicate a subtle confinement effect on the conformation of S1 in ZIF-8 that ultimately influences the observed HFIs. However, the magnitude of the difference observed between S1@ZIF and S1 in *n*-pentane is comparable to the accuracy of measurements. Thus, we provide the first experimental evidence that the internal surface of the ZIF-8 cavity sensed by guest molecules is strongly non-polar, in perfect agreement with theoretical expectations for this structure and with the analysis of water vapor sorption isotherms.[23,27]

3.2. Nanoscale ordering of solvents in ZIF-8 cavities

Next, it would be useful to measure the apparent polarity of the MOF interior when guest solvent molecules are present in the cavities. Lot of current research concerns chemical/catalytic reactions occurring inside MOFs;[57–60] therefore such information is very much needed.

As an example, Fig. 3 shows CW EPR of S1@ZIF-8 impregnated with different alcohols. The empty cavity of ZIF-8 can accommodate 8–10 molecules of alcohols; however, in the presence of nitroxide in the same cavity, this number can be reduced to ~4–5. The spectra are markedly different, and the obtained HFI constants are listed in Table 1.

However, the most astonishing observation is that apparent polarity sensed by the spin probe inside ZIF-8 impregnated with alcohols differs from that in the corresponding bulk alcohols in a peculiar way. Fig. 4a shows the A_N and A_P values *vs.* Reichardt polarity E_N^T for ZIF-8 impregnated with a set of solvents, as well as for the same bulk solvents. The A_N values change very insignificantly with E_N^T, and there is also no solid trend between A_N in the impregnated MOF and in bulk solvent. At the same time, the A_P values change noticeably *vs.* E_N^T, and they are markedly different in the MOF *vs.* bulk. Note that the other non-hydrogen bonding solvents show the same trend (see more data in the ESI†).

Fig. 4a can be understood in a way that the polarity sensed *via* A_P is much higher in impregnated ZIF-8 compared to the

Table 1 Isotropic HFI constants for S1 in different environments (pure solvents, bare ZIF-8, or ZIF-8 impregnated with various solvents, as indicated in the left column). The errors of A_N and A_P measurements were set by a comparison of the results of the present work and ref. 34 in water. TFE is 2,2,2-trifloroethanol. E_N^T is the Reichardt polarity constant, θ is the dihedral angle shown in Fig. 1c, V_X and V_M – intrinsic and molar volumes, and c – cohesive pressure (see the text for more details). The last column shows reference numbers used for the corresponding media in Fig. 6

Environment	A_N/mT ±0.040 mT	A_P/mT ±0.050 mT	E_N^T	θ	V_X	V_M	c	No.
Water	1.612	2.231			16.7			
	1.650 (ref. 52)	2.280 (ref. 52)	1.000 (ref. 51)	54		18	2294	
ZIF-8	1.420	4.033		34				1
n-Pentane	1.406 (ref. 51)	4.135 (ref. 51)	0.009 (ref. 51)	34	81.3	114.52	205	
ZIF-8 + isopropanol	1.514	2.271		53				2
Isopropanol	1.520 (ref. 61)	2.760 (ref. 61)	0.546 (ref. 51)	50	59	76.51	558	
ZIF-8 + propanol-1	1.520	2.038		55				3
Propanol-1	1.525	2.453	0.617 (ref. 51)	51	59	74.8	600	
ZIF-8 + ethanol	1.535	1.840		58				4
Ethanol	1.560 (ref. 61)	2.400 (ref. 61)	0.654 (ref. 51)	52	44.9	58.41	676	
ZIF-8 + methanol	1.543	1.543		61				5
Methanol	1.570 (ref. 61)	2.190 (ref. 61)	0.762 (ref. 51)	55	30.8	40.43	858	
ZIF-8 + ethylene glycol	1.565	1.470		62				6
Ethylene glycol	1.540 (ref. 51)	2.159 (ref. 51)	0.790 (ref. 51)	54	50.8	56.01	1050	
ZIF-8 + TFE	1.560	1.430		62				7
TFE	1.590 (ref. 51)	2.042 (ref. 51)	0.898 (ref. 51)	56	41.5	72.4	573	

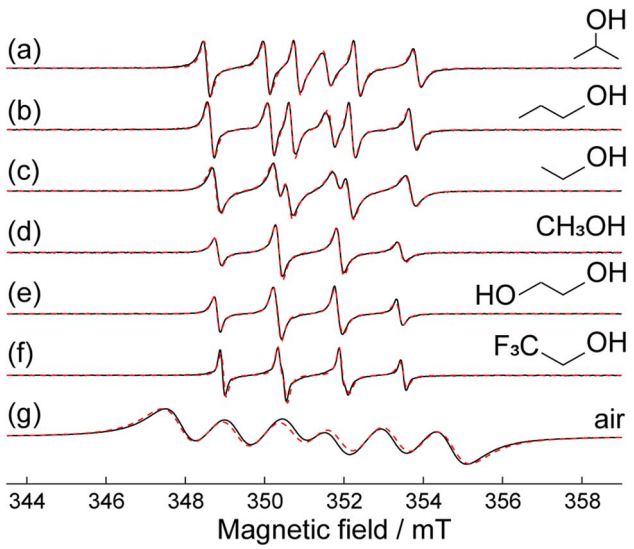

Fig. 3 X-band room-temperature CW EPR spectra of S1@ZIF-8 impregnated by: isopropanol (a), propanol-1 (b), ethanol (c), methanol (d), ethylene glycol (e), and 2,2,2-trifluoroethanol (f). For reference, the solvent-free S1@ZIF-8 filled with atmospheric air is shown in (g). Experimental spectra are shown as solid black lines and simulations as dotted red lines.

same bulk solvent. At the same time, A_N shows the same trend only for some solvents, and the results based on A_N are inconclusive. In fact, they fall within the uncertainty introduced by a minor confinement effect discussed above on the basis of comparison with *n*-pentane (~0.06 mT). Thus, we should hold to the more reliable data delivered by A_P, whose dependence on solvent polarity spreads over a much broader range.

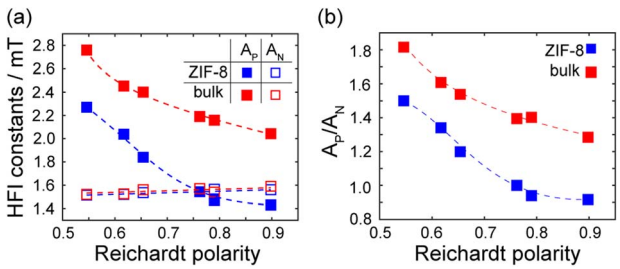

Fig. 4 (a) A_N and A_P values *vs.* Reichardt polarity E_N^T in the bulk and in ZIF-8. (b) A_P/A_N ratio *vs.* E_N^T in the bulk (red) and in ZIF-8 (blue). The lines guide the eye.

The electron density on the phosphorus atom originates from the hyperconjugation mechanism, which depends on the angle θ shown in Fig. 1c *via* the Heller–McConnell relationship:

$$A_P = B_0 + B_1\rho_N^\pi \cos^2\theta \approx B_1 A_N \cos^2\theta \quad (1)$$

Fig. 4b shows the ratio A_P/A_N *vs.* E_N^T, which can be understood using eqn (1) as indirect dependence of θ on E_N^T. As is shown in Fig. 4b, the dependence of A_N and A_P in the MOF is more pronounced than in the bulk, implying that angle θ changes more *vs.* solvent polarity for radical encapsulated in the MOF.

One might think that the confinement of radicals in the MOF filled with the solvent imposes steric hindrance leading to specific distortions of radical geometry and amplification of angle θ in the MOF compared to the corresponding bulk solvent. However, if pronounced steric hindrances take place, one would simultaneously expect more restricted and potentially anisotropic mobility of the radical. However, all EPR

spectra shown in Fig. 3 have the lineshapes close to the isotropic limit, which implies that the rotation of the radical is rather fast and thus not strongly constrained. Recently, we have shown that TEMPO nitroxide exhibits slightly anisotropic mobility at room temperatures being confined in ZIF-8 impregnated with alcohols.[62] However, despite some anisotropy of rotation imposed by the cavity partly occupied by solvent molecules, the observed rotational correlation times were rather short (<130 ps). Thus, as long as the single set of HFI couplings is observed, one can assume that the values of these couplings correctly reflect the apparent polarity of the MOF cavity.

The most evident difference between bulk and in-MOF A_P values is found for methanol, where we observe $A_N = A_P = 1.543$ mT for S1@ZIF-8 and $[A_N, A_P] = [1.570, 2.190]$ mT for S1 in bulk methanol. The nitrogen HFI A_N is nearly the same (within given accuracy) in both cases, whereas phosphorus HFI A_P is dramatically smaller in the MOF. In fact, such a small value $A_P = 1.543$ mT was not obtained in any bulk organic solvent, even in water.[63,64]

The decrease in A_p (Fig. 4a) is dependent on the dihedral angle θ (eqn (1)) and denotes that conformer **B** is favored over conformer **A** in a polar environment due to its $N^{+\bullet}$—$O^{-}\cdots P^{+}$—O^{-} dipole–dipole interaction (see Fig. 1c). We suggest there are two plausible mechanisms that can explain larger apparent polarity (larger θ) obtained in ZIF-8 impregnated with solvents compared to the same bulk solvents. Both mechanisms assume that the ZIF-8 cavity introduces nanoordering of solvent molecules, which preferentially cover the walls of the cavities (the latter is well justified by rather fast and isotropic rotation of the radical, as was discussed above).

First the 'structuredness-driven' mechanism involves interplay between the polarity and factors such as solvent organization given by the molar volume V_M. The reorganization of solvent forced by the ZIF cavity leads to a striking increase of the organization of the cybotactic layer depending on the size of the solvent. Therefore, solvent molecules covering the cavity walls (higher structuredness) cause the release of constraints around the C–P bond of a radical compared to the bulk solvent, thus affording easier rotation (lower stiffness) and favoring conformer **B** (larger θ). This loss of organization is balanced with the increase of the size, which reduces the space in the cavity (as given by the negative value of the parameter, see below). Once there are polar solvent molecules in the cavity of ZIF-8, they impose electric fields on a radical (favoring conformer **B**), but at the same time do not provide as strong steric constraints as the same molecules in the bulk, resulting in larger θ values compared to those in the same bulk solvent.

The second 'hyperpolarity' mechanism relies on the fact that alcohols, for example methanol, are composed of a hydrophobic part (alkyl fragment) and a hydrophilic part (OH function). Therefore, it is plausible that guest molecules inside the cavity of a MOF are nanoordered in a way that non-polar (hydrophobic) moieties are directed towards the cavity walls, while polar moieties are directed towards the cavity center (sketched in Fig. 5). In this case, the electric field imposed onto a radical in the MOF impregnated with solvent (*e.g.* methanol) can be higher than that in the bulk, where all solvent molecules around the radical are disordered, thus leading to a higher apparent polarity ('hyperpolarity') sensed by the radical. We attempted to confirm this mechanism using pulse EPR (ESEEM) and partly deuterated methanol; however, the observed trend was too weak to provide ultimate experimental proof (see the ESI†).

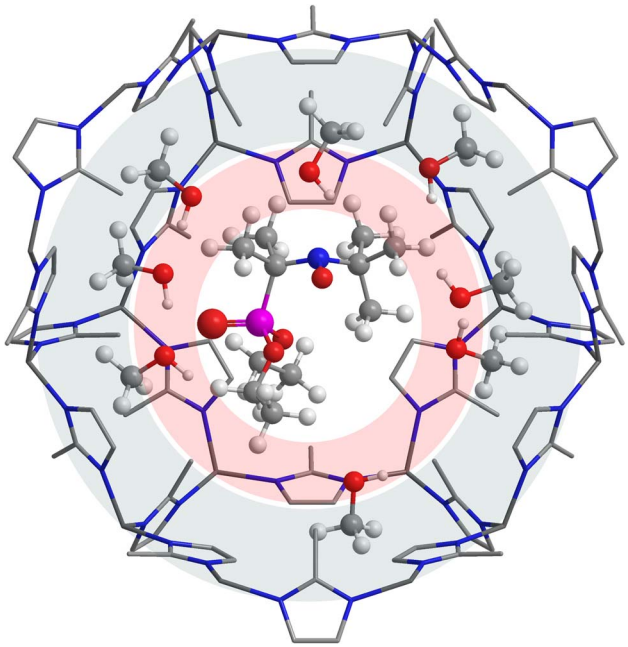

Fig. 5 Proposed methanol localization in the cavity of S1@ZIF-8. Hydrophilic environment around the probe is shaded in red, whereas the hydrophobic part of the cavity is marked in gray.

In fact, both mechanisms can work simultaneously; however, let us briefly discuss the pros and cons of each one in view of available experimental data.

When other alcohols are used (ethanol, isopropanol, ethylene glycol, and TFE), the apparent polarity inside the cavity sensed by a phosphorus HFI (A_P) progressively decreases (A_P increases) (Table 1). This trend follows the one for bulk solvents; but still the apparent polarity in the cavity is systematically larger than that in the bulk solvent. The decrease of the apparent polarity in the order methanol > ethanol > isopropanol agrees well with the qualitative expectations that the ratio of polar/non-polar moieties in these molecules decreases. In this case, even though ordering of solvent molecules in the MOF is still effective (leading to a higher polarity *vs.* the corresponding bulk solvent), the apparent polarity can be comparable to that in some common organic solvents (though different from the impregnating one). At the same time, the volume of solvent molecules grows in the order isopropanol > ethanol > methanol, implying possible increase of steric hindrances for the rotation around the C–N bond and inhibiting large θ-values. Therefore, the trends observed for a series of alcohols are consistent with both structuredness-driven and hyperpolarity mechanisms.

Let us consider in more detail the absolute values of the observed spectroscopic parameters. Assuming $B_1\rho_N^{\pi} = 5.9$ mT in non-polar solvent such as pentane,[51–55] the corresponding θ

value can be estimated as 34° based on eqn (1), both in bulk pentane and in solvent-free ZIF-8. To determine θ in other solvents, changes in ρ_N^{π} due to the change in the polarity of solvent are accounted by assuming $\rho_N^{\pi} \approx A_N$. Thus, θ is given by eqn (2) ($A_{P,pentane}$ and $A_{N,pentane}$ refer to the ^{31}P and ^{14}N HFI constants in bulk *n*-pentane, respectively, whereas $A_{P,n}$ and $A_{N,n}$ stand for similar values in the arbitrary case; $\theta_{pentane}$ is given by eqn (1)).

$$\cos\theta_n = \sqrt{\frac{A_{p,n}}{A_{p,pentane}} \cdot \frac{A_{N,pentane}}{A_{N,n}}} \cos\theta_{pentane} \quad (2)$$

Previously, it has been shown that A_N and A_P values can be described using multiparameter Kamlet–Abboud–Taft and Koppel–Palm equations, which take into account polarity, H-bonding, bulk/cavity terms given by the structuredness/stiffness, and volume of solvent (c, V_X or V_M, respectively).[52–55] Due to the small number of solvents investigated (see Table 1), the KAT relationship is preferred in the form where polarity and H-bonding are accounted in Reichardt constant E_T^N, reducing the number of parameters. It is combined, in eqn (3), with the molar volume V_M, which provides the best correlation (see the ESI†) describing the bulk/cavity effect (Fig. 6 and eqn (4)): E_T^N ($N = 11$, t-test at 99.99% for θ_0, at 99.88% for E_T^N, and at 99.52% for V_M, $R^2 = 0.976$, $F = 165$, and F-test at 99.99%).

$$\theta = \theta_0 + a_1 E_T^N + a_4 V_M \quad (3)$$

$$\theta = 53.1(\pm1.7) + 19.4(\pm2.8)\cdot E_T^N - 0.13(\pm0.03)\cdot V_M \quad (4)$$

Fig. 6 shows that the combination of the Reichardt polarity constant E_T^N and cohesive pressure V_M allows for good linear correlation with the observed θ values. This means that the observed anomalous HFI constants in ZIF-8 impregnated with solvents stem from both structuredness-driven and hyperpolarity mechanisms. Their relative contributions are different for different solvents. Although the detailed analysis is still to be done in the future, based on the values reported in Table 1 we conclude that the second mechanism dominates for the studied set of solvents. It is noteworthy that both mechanisms rely on the solvent ordering in the cavities, which favors the **B** conformer much stronger in-MOF compared to the same bulk solvents.

To confirm that the rotation around the C–N bond (Fig. 1c) is the major factor influencing A_P values, we performed a series of DFT calculations (see the ESI†). We calculated the dependence of A_P on $\cos^2\theta$ upon variations of other geometric parameters (bond lengths, angles, and dihedrals). In all cases, the correlation between A_P and $\cos^2\theta$ was maintained, and the deviations were smaller than the changes of A_P *vs.* θ.

Remarkably, the observed solvent ordering is an important effect for carrying out the reactions in ZIF-8, since the structure and properties (such as polarity) of the active site environment might be decisive for the enhancement/inhibition of particular reaction routes. Moreover, polarity-dependent stabilization of certain transition states has high impact on the efficiency of enzymatic reactions and selective catalysts.[65–69] Therefore, we believe that this finding is extremely important for understanding chemical reactions occurring in MOFs and must be taken into consideration when such particular applications are being designed.

3.3. Multiple conformations of β-phosphorylated nitroxide in ZIF-8

In all cases discussed above, when ZIF-8 cavities with β-phosphorylated nitroxide S1 were impregnated with a particular solvent, we observed the EPR spectra characterized by a single set of HFI constants A_P and A_N. However, in some cases we also observed spectra, which can be described only using two or more sets of HFI values. For example, this is very clear for S1@ZIF-8 impregnated with *n*-hexane (Fig. 7a). Such a spectrum can be simulated only assuming two sets of HFI constants listed in Tables 2 and S5 (ESI).†

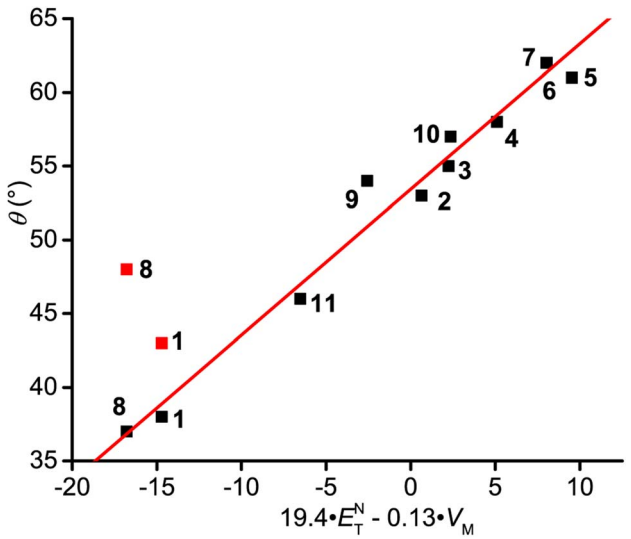

Fig. 6 Plot of dihedral angle θ *vs.* $f(E_N^T, V_M)$ given by eqn (4).

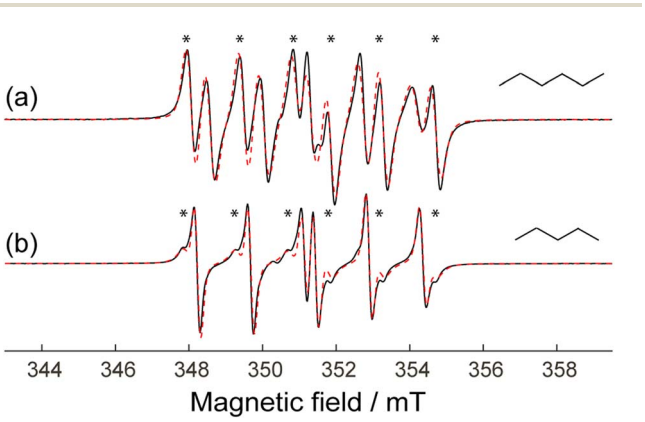

Fig. 7 X-band room-temperature CW EPR spectra of S1@ZIF-8 in the presence of: *n*-hexane (a) and *n*-pentane (b). Experimental spectra are shown as solid black lines and simulations as dotted red lines. Signals from minor conformation in each case are marked with asterisks.

Table 2 Isotropic HFI constants for S1 in different environments yielding two conformations of the S1 radical

Environment	A_N/mT ± 0.040 mT	A_P/mT ± 0.050 mT	Fraction
ZIF-8 + *n*-hexane	1.431	3.798	0.45
	1.465	2.723	0.55
n-Hexane	1.430 (ref. 61)	4.168 (ref. 61)	
ZIF-8 + *n*-pentane	1.431	3.798	0.45
	1.462	3.218	0.55
n-Pentane	1.406 (ref. 61)	4.135 (ref. 61)	

In both cases we have obtained very close values for minor components (*n*-pentane: $A_N = 1.431$ mT and $A_P = 3.650$ mT; *n*-hexane: $A_N = 1.431$ mT and $A_P = 3.798$ mT). Moreover these values of A_N and A_P are close to those observed in the corresponding non-polar bulk solvents. At the same time, the sets of parameters for the major components have noticeably different values of A_P in *n*-hexane and *n*-pentane, while A_N values are closely the same. Therefore, we speculate that for each of two above solvents there are two local surroundings of the radical in the ZIF-8 cavity: one that does not impose steric hindrances leading to enforced conformation and another one that does impose such hindrances. Most plausibly, the latter situation refers to the cavities with a larger number of solvent molecules inside compared to the former one. In addition, when we deal with a 'tighter' radical surrounding, the resulting enforced conformation should naturally depend on the structure of solvent. This explains why the second (major, enforced) components of the spectra are described by different HFIs for *n*-pentane and *n*-hexane, while the first ones (minor, unperturbed) are rather close.

In summary, the above consideration shows that the minor components of these complex two-component EPR spectra reflect the polarity and structuredness of the radical environment, whereas the major components refer to 'unnatural' radical conformations enforced by severe steric hindrances. In principle, in a systematic study the component of interest can be safely identified and interpreted.

4. Conclusions and outlook

In this work, we proposed and validated a new approach for the investigation of the internal surface of MOF cavities using β-phosphorylated nitroxides and EPR spectroscopy. These radical probes can be entrapped in trace amounts inside the cavities of the MOF during synthesis and provide a plethora of unique information. This approach is applicable for both bare MOFs and MOFs with adsorbed/impregnated guest molecules. In particular, hyperfine interaction constants on ^{14}N and ^{31}P nuclei of the radical are highly sensitive to local polarity; therefore such radical@MOF materials allow obtaining values of local apparent polarity in MOF cavities *in situ* under relevant conditions.

All these benefits were demonstrated using one of the most appealing MOFs nowadays – ZIF-8. Exploiting the radical sensitive to a microenvironment we have experimentally evidenced that the ZIF-8 cavity is non-polar. Also, we determined that impregnation of ZIF-8 with different alcohols leads to a drastic change in the apparent polarity inside the cavity (*i.e.* a polarity sensed by solutes) from non-polar to a highly polar one. Remarkably, in the cases of methanol, ethanol and isopropanol, the apparent polarity inside ZIF-8 was found to be higher than that in the bulk solvent. In the cases of methanol and ethanol, it is even higher than that in any bulk organic solvent. This was rationalized by nanoordering of alcohol molecules inside the cavity of ZIF-8 driven by hydrophobic interactions.

Many applications of MOFs require their impregnation with a solution of reactants, which is especially true for the MOF catalysis.[70–74] Moreover, the design of chemical processes in MOFs needs understanding of local properties, in particular the polarities of MOF internal surfaces sensed by solutes and carrier solvents, as well as the structuredness of the corresponding cybotactic layers. As is shown in the present work, the values of apparent polarity inside MOFs and local solvent organization can be drastically different from expectations based on the bulk properties of the same molecules, and this needs to be carefully accounted for in the future. The methodology developed by us has a broad scope of applications, and it is quite easy to implement and provides a lot of opportunities for understanding and rational optimization of chemical reactions in MOFs. In this work it was exemplified using ZIF-8; however, the properties of many other MOFs (for instance, other MOFs of the ZIF family and recent example of UiO-66 (ref. 50)) can be accessed in the same way. Therefore, we believe that the methodology and conclusions of this paper may find broad implementation in MOF science in the future.

Data availability

The datasets supporting this article have been uploaded as part of the ESI.†

Author contributions

Conceptualization and methodology: A. S. P., R. Z. S., S. R. A. M. and M. V. F.; investigation: A. S. P., A. A. E., D. V. A., K. A. S., D. M. P., and S. J.; writing—original draft preparation: A. S. P., S. R. A. M., and M. V. F.; writing—review and editing: S. R. A. M. and M. V. F.; supervision: S. R. A. M. and M. V. F. All authors have read and agreed to the published version of the manuscript.

Conflicts of interest

There are no conflicts to declare.

Acknowledgements

This work was supported by the Russian Science Foundation (No. 22-73-10239, EPR studies). We thank the Ministry of Science and Higher Education of the Russian Federation for

granting access to the equipment. Support from ANR-20-CE06-0006-04 is greatly acknowledged.

Notes and references

1 O. M. Yaghi, G. Li and H. Li, *Nature*, 1995, **378**, 703–706.
2 P. I. Scheurle, A. Mähringer, A. C. Jakowetz, P. Hosseini, A. F. Richter, G. Wittstock, D. D. Medina and T. Bein, *Nanoscale*, 2019, **11**, 20949–20955.
3 J. N. Hao and B. Yan, *Nanoscale*, 2016, **8**, 2881–2886.
4 Z. Wang, M. Gui, M. Asif, Y. Yu, S. Dong, H. Wang, W. Wang, F. Wang, F. Xiao and H. Liu, *Nanoscale*, 2018, **10**, 6629–6638.
5 T. M. McDonald, J. A. Mason, X. Kong, E. D. Bloch, D. Gygi, A. Dani, V. Crocellà, F. Giordanino, S. O. Odoh, W. S. Drisdell, B. Vlaisavljevich, A. L. Dzubak, R. Poloni, S. K. Schnell, N. Planas, K. Lee, T. Pascal, L. F. Wan, D. Prendergast, J. B. Neaton, B. Smit, J. B. Kortright, L. Gagliardi, S. Bordiga, J. A. Reimer and J. R. Long, *Nature*, 2015, **519**, 303–308.
6 X. Zhang, Z. Huang, M. Ferrandon, D. Yang, L. Robison, P. Li, T. C. Wang, M. Delferro and O. K. Farha, *Nat. Catal.*, 2018, **1**, 356–362.
7 D. Yang and B. C. Gates, *ACS Catal.*, 2019, **9**, 1779–1798.
8 C. S. Diercks, Y. Liu, K. E. Cordova and O. M. Yaghi, *Nat. Mater.*, 2018, **17**, 301–307.
9 J. E. Ellis, Z. Zeng, S. I. Hwang, S. Li, T. Y. Luo, S. C. Burkert, D. L. White, N. L. Rosi, J. J. Gassensmith and A. Star, *Chem. Sci.*, 2019, **10**, 737–742.
10 J. López-Cabrelles, E. Miguel-Casañ, M. Esteve-Rochina, E. Andres-Garcia, I. J. Vitórica-Yrezábal, J. Calbo and G. Mínguez Espallargas, *Chem. Sci.*, 2022, **13**, 842–847.
11 T. Wang, Y. Wang, M. Sun, A. Hanif, H. Wu, Q. Gu, Y. S. Ok, D. C. W. Tsang, J. Li, J. Yu and J. Shang, *Chem. Sci.*, 2020, **11**, 6670–6681.
12 A. Phan, C. J. Doonan, F. J. Uribe-Romo, C. B. Knobler, M. O'Keeffe and O. M. Yaghi, *Acc. Chem. Res.*, 2010, **43**, 58–67.
13 K. S. Park, Z. Ni, A. P. Côté, J. Y. Choi, R. Huang, F. J. Uribe-Romo, H. K. Chae, M. O'Keeffe and O. M. Yaghi, *Proc. Natl. Acad. Sci. U. S. A.*, 2006, **103**, 10186–10191.
14 A. Noguera-Díaz, J. Villarroel-Rocha, V. P. Ting, N. Bimbo, K. Sapag and T. J. Mays, *J. Chem. Technol. Biotechnol.*, 2019, **94**, 3787–3792.
15 D. Fairen-Jimenez, S. A. Moggach, M. T. Wharmby, P. A. Wright, S. Parsons and T. Düren, *J. Am. Chem. Soc.*, 2011, **133**, 8900–8902.
16 Y. Pan, Y. Liu, G. Zeng, L. Zhao and Z. Lai, *Chem. Commun.*, 2011, **47**, 2071.
17 S. Yan, D. Zhu, Z. Zhang, H. Li, G. Chen and B. Liu, *Appl. Energy*, 2019, **248**, 104–114.
18 S. R. Venna and M. A. Carreon, *J. Am. Chem. Soc.*, 2010, **132**, 76–78.
19 A. Knebel, B. Geppert, K. Volgmann, D. I. Kolokolov, A. G. Stepanov, J. Twiefel, P. Heitjans, D. Volkmer and J. Caro, *Science*, 2017, **358**, 347–351.
20 K. Zhang, R. P. Lively, C. Zhang, R. R. Chance, W. J. Koros, D. S. Sholl and S. Nair, *J. Phys. Chem. Lett.*, 2013, **4**, 3618–3622.
21 K. Zhang, R. P. Lively, C. Zhang, R. R. Chance, W. J. Koros, D. S. Sholl and S. Nair, *J. Phys. Chem. Lett.*, 2013, **4**, 3618–3622.
22 P. Z. Moghadam, D. Fairen-Jimenez and R. Q. Snurr, *J. Mater. Chem. A*, 2016, **4**, 529–536.
23 J. Cousin Saint Remi, T. Rémy, V. Van Hunskerken, S. van de Perre, T. Duerinck, M. Maes, D. De Vos, E. Gobechiya, C. E. A. Kirschhock, G. V. Baron and J. F. M. Denayer, *ChemSusChem*, 2011, **4**, 1074–1077.
24 Z. Abbasi, E. Shamsaei, X.-Y. Fang, B. Ladewig and H. Wang, *J. Colloid Interface Sci.*, 2017, **493**, 150–161.
25 K. Jayaramulu, K. K. R. Datta, C. Rösler, M. Petr, M. Otyepka, R. Zboril and R. A. Fischer, *Angew. Chem., Int. Ed.*, 2016, **55**, 1178–1182.
26 K.-Y. A. Lin, Y.-C. Chen and S. Phattarapattamawong, *J. Colloid Interface Sci.*, 2016, **478**, 97–106.
27 A. U. Ortiz, A. P. Freitas, A. Boutin, A. H. Fuchs and F.-X. Coudert, *Phys. Chem. Chem. Phys.*, 2014, **16**, 9940–9949.
28 B. Jee, P. St. Petkov, G. N. Vayssilov, T. Heine, M. Hartmann and A. Pöppl, *J. Phys. Chem. C*, 2013, **117**, 8231–8240.
29 M. Šimėnas, B. Jee, M. Hartmann, J. Banys and A. Pöppl, *J. Phys. Chem. C*, 2015, **119**, 28530–28535.
30 A. S. Poryvaev, A. M. Sheveleva, P. A. Demakov, S. S. Arzumanov, A. G. Stepanov, D. N. Dybtsev and M. V. Fedin, *Appl. Magn. Reson.*, 2018, **49**, 255–264.
31 S. A. Sapchenko, M. O. Barsukova, R. V. Belosludov, K. A. Kovalenko, D. G. Samsonenko, A. S. Poryvaev, A. M. Sheveleva, M. V. Fedin, A. S. Bogomyakov, D. N. Dybtsev, M. Schröder and V. P. Fedin, *Inorg. Chem.*, 2019, **58**, 6811–6820.
32 M. Mendt, F. Gutt, N. Kavoosi, V. Bon, I. Senkovska, S. Kaskel and A. Pöppl, *J. Phys. Chem. C*, 2016, **120**, 14246–14259.
33 M. Mendt, P. Vervoorts, A. Schneemann, R. A. Fischer and A. Pöppl, *J. Phys. Chem. C*, 2019, **123**, 2940–2952.
34 M. Mendt, B. Jee, N. Stock, T. Ahnfeldt, M. Hartmann, D. Himsl and A. Pöppl, *J. Phys. Chem. C*, 2010, **114**, 19443–19451.
35 A. S. Poryvaev, A. M. Sheveleva, D. I. Kolokolov, A. G. Stepanov, E. G. Bagryanskaya and M. V. Fedin, *J. Phys. Chem. C*, 2016, **120**, 10698–10704.
36 A. M. Sheveleva, D. I. Kolokolov, A. A. Gabrienko, A. G. Stepanov, S. A. Gromilov, I. K. Shundrina, R. Z. Sagdeev, M. V. Fedin and E. G. Bagryanskaya, *J. Phys. Chem. Lett.*, 2014, **5**, 20–24.
37 T. Wang, L. Gao, J. Hou, S. J. A. Herou, J. T. Griffiths, W. Li, J. Dong, S. Gao, M.-M. Titirici, R. V. Kumar, A. K. Cheetham, X. Bao, Q. Fu and S. K. Smoukov, *Nat. Commun.*, 2019, **10**, 1340.
38 W. G. Cui, G. Y. Zhang, T. L. Hu and X. H. Bu, *Coord. Chem. Rev.*, 2019, **387**, 79–120.
39 B. An, Z. Li, Y. Song, J. Zhang, L. Zeng, C. Wang and W. Lin, *Nat. Catal.*, 2019, **28**(2), 709–717.
40 B. Jee, K. Koch, L. Moschkowitz, D. Himsl, M. Hartman and A. Pöppl, *J. Phys. Chem. Lett.*, 2011, **2**, 357–361.
41 A. M. Sheveleva, A. V. Anikeenko, A. S. Poryvaev, D. L. Kuzmina, I. K. Shundrina, D. I. Kolokolov,

A. G. Stepanov and M. V. Fedin, *J. Phys. Chem. C*, 2017, **121**, 19880–19886.
42 X. Han, H. G. W. Godfrey, L. Briggs, A. J. Davies, Y. Cheng, L. L. Daemen, A. M. Sheveleva, F. Tuna, E. J. L. McInnes, J. Sun, C. Drathen, M. W. George, A. J. Ramirez-Cuesta, K. M. Thomas, S. Yang and M. Schröder, *Nat. Mater.*, 2018, **17**, 691–696.
43 D. M. Polyukhov, A. S. Poryvaev, S. A. Gromilov and M. V. Fedin, *Nano Lett.*, 2019, **19**, 6506–6510.
44 A. S. Poryvaev, A. A. Yazikova, D. M. Polyukhov and M. V. Fedin, *Microporous Mesoporous Mater.*, 2022, **330**, 111564.
45 D. M. Polyukhov, A. S. Poryvaev, A. S. Sukhikh, S. A. Gromilov and M. V. Fedin, *ACS Appl. Mater. Interfaces*, 2021, **13**, 40830–40836.
46 N. A. Kudryavyh, M. Y. Ivanov, A. S. Poryvaev, D. M. Polyukhov, R. Z. Sagdeev and M. V. Fedin, *Dokl. Phys. Chem.*, 2023, **509**, 57–63.
47 A. A. Efremov, A. S. Poryvaev, D. M. Polyukhov and M. V. Fedin, *Microporous Mesoporous Mater.*, 2022, **332**, 111713.
48 A. S. Poryvaev, D. M. Polyukhov and M. V. Fedin, *ACS Appl. Mater. Interfaces*, 2020, **12**, 16655–16661.
49 M. V. Fedin, *Russ. Chem. Bull.*, 2023, **722**(72), 312–334.
50 A. S. Poryvaev, K. P. Larionov, Y. N. Albrekht, A. A. Efremov, A. S. Kiryutin, K. A. Smirnova, V. Y. Evtushok and M. V. Fedin, *Phys. Chem. Chem. Phys.*, 2023, **25**, 13846–13853.
51 G. Audran, P. Brémond, S. R. A. Marque and G. Obame, *ChemPhysChem*, 2012, **13**, 3542–3548.
52 G. Audran, L. Bosco, P. Brémond, T. Butscher, J. M. Franconi, S. R. A. Marque, P. Mellet, E. Parzy, M. Santelli and E. Thiaudière, *Org. Biomol. Chem.*, 2015, **13**, 11393–11400.
53 G. Audran, L. Bosco, P. Brémond, T. Butscher and S. R. A. Marque, *Org. Biomol. Chem.*, 2016, **14**, 1288–1292.
54 G. Audran, L. Bosco, P. Brémond, T. Butscher, J. M. Franconi, K. Kabitaev, S. R. A. Marque, P. Mellet, E. Parzy, M. Santelli, E. Thiaudière and S. Viel, *RSC Adv.*, 2016, **6**, 5653–5670.
55 P. Nkolo, G. Audran, P. Bremond, R. Bikanga, S. R. A. Marque and V. Roubaud, *Tetrahedron*, 2017, **73**, 3188–3201.
56 S. Stoll and A. Schweiger, *J. Magn. Reson.*, 2006, **178**, 42–55.
57 L. Jiao, Y. Wang, H.-L. Jiang and Q. Xu, *Adv. Mater.*, 2018, **30**, 1703663.
58 T. Wang, L. Gao, J. Hou, S. J. A. Herou, J. T. Griffiths, W. Li, J. Dong, S. Gao, M.-M. Titirici, R. V. Kumar, A. K. Cheetham, X. Bao, Q. Fu and S. K. Smoukov, *Nat. Commun.*, 2019, **10**, 1340.
59 D. Jiang, G. Fang, Y. Tong, X. Wu, Y. Wang, D. Hong, W. Leng, Z. Liang, P. Tu, L. Liu, K. Xu, J. Ni and X. Li, *ACS Catal.*, 2018, **8**, 11973–11978.
60 A. D. Cardenal, H. Jeong Park, C. J. Chalker, K. G. Ortiz and D. C. Powers, *Chem. Commun.*, 2017, **53**, 7377–7380.
61 S. R. A. Marque, G. Audran and J. Patrick Joly, *J. Chem. Eng. Bioanal. Chem.*, 2018, **2**, 70–76.
62 A. A. Efremov, A. S. Poryvaev, D. M. Polyukhov, R. Z. Sagdeev and M. V. Fedin, *Appl. Magn. Reson.*, 2022, 1–13.
63 G. Audran, P. Brémond, S. R. A. Marque and G. Obame, *ChemPhysChem*, 2012, **13**, 3542–3548.
64 A. S. Mukhtarov, A. V. Il'yasov, Y. A. Levin, I. P. Gozman, M. S. Skorobogatova and E. I. Zoroatskaya, *Theor. Exp. Chem.*, 1976, **12**, 656–660.
65 A. Nicolas, M. Egmond, C. T. Verrips, J. de Vlieg, S. Longhi, C. Cambillau and C. Martinez, *Biochemistry*, 1996, **35**, 398–410.
66 S. A. Meadows, C. Y. Edosada, M. Mayeda, T. Tran, C. Quan, H. Raab, C. Wiesmann and B. B. Wolf, *Biochemistry*, 2007, **46**, 4598–4605.
67 P. J. Dyson and P. G. Jessop, *Catal. Sci. Technol.*, 2016, **6**, 3302–3316.
68 B. W. Bakr and C. D. Sherrill, *Phys. Chem. Chem. Phys.*, 2016, **18**, 10297–10308.
69 B. W. Bakr and C. D. Sherrill, *Phys. Chem. Chem. Phys.*, 2018, **20**, 18241–18251.
70 A. Schejn, A. Aboulaich, L. Balan, V. Falk, J. Lalevée, G. Medjahdi, L. Aranda, K. Mozet and R. Schneider, *Catal. Sci. Technol.*, 2015, **5**, 1829–1839.
71 M. Lammert, M. T. Wharmby, S. Smolders, B. Bueken, A. Lieb, K. A. Lomachenko, D. De Vos and N. Stock, *Chem. Commun.*, 2015, **51**, 12578–12581.
72 A. Dhakshinamoorthy, A. Santiago-Portillo, A. M. Asiri and H. Garcia, *ChemCatChem*, 2019, **11**, 899–923.
73 C. Kutzscher, G. Nickerl, I. Senkovska, V. Bon and S. Kaskel, *Chem. Mater.*, 2016, **28**, 2573–2580.
74 A. Iglesias-Juez, S. Castellanos, M. Monte, G. Agostini, D. Osadchii, M. A. Nasalevich, J. G. Santaclara, A. I. Olivos Suarez, S. L. Veber, M. V. Fedin and J. Gascón, *J. Mater. Chem. A*, 2018, **6**, 17318–17322.